

# THE S<sup>4</sup>G PERSPECTIVE ON CIRCUMSTELLAR DUST EXTINCTION OF AGB STARS IN M100

SHARON E. MEIDT<sup>1</sup>, EVA SCHINNERER<sup>1</sup>, JUAN-CARLOS MUÑOZ-MATEOS<sup>2</sup>, BENNE HOLWERDA<sup>3</sup>, LUIS C. HO<sup>4</sup>, BARRY F. MADORE<sup>4</sup>, JOHAN H. KNAPEN<sup>5,6</sup>, ALBERT BOSMA<sup>7</sup>, E. ATHANASSOULA<sup>7</sup>, JOANNAH L. HINZ<sup>8</sup>, KARTIK SHETH<sup>4,9,10</sup>, MICHAEL REGAN<sup>11</sup>, ARMANDO GIL DE PAZ<sup>12</sup>, KARÍN MENÉNDEZ-DELMESTRE<sup>4</sup>, MARK SEIBERT<sup>4</sup>, TAEHYUN KIM<sup>2</sup>, TRISHA MIZUSAWA<sup>9,10</sup>, DIMITRI A. GADOTTI<sup>13</sup>, ELJA LAURIKAINEN<sup>14,15</sup>, HEIKKI SALO<sup>14</sup>, JARKKO LAINE<sup>14,15</sup>, SÉBASTIEN COMERÓN<sup>16</sup>

(Dated: December 6, 2021)  
Draft version December 6, 2021

## ABSTRACT

We examine the effect of circumstellar dust extinction on the near-IR contribution of asymptotic giant branch (AGB) stars in intermediate-age clusters throughout the disk of M100. For our sample of 17 AGB-dominated clusters we extract optical-to-mid-IR SEDs and find that NIR brightness is coupled to the mid-IR dust emission in such a way that a significant reduction of AGB light, of up to 1 mag in K-band, follows from extinction by the dust shell formed during this stage. Since the dust optical depth varies with AGB chemistry (C-rich or O-rich), our results suggest that the contribution of AGB stars to the flux from their host clusters will be closely linked to the metallicity and the progenitor mass of the AGB star, to which dust chemistry and mass-loss rate are sensitive. Our sample of clusters—each the analogue of a  $\sim 1$  Gyr old post-starburst galaxy—has implications within the context of mass and age estimation via SED modelling at high  $z$ : we find that the average  $\sim 0.5$  mag extinction estimated here may be sufficient to reduce the AGB contribution in (rest-frame) K-band from  $\sim 70\%$ , as predicted in the latest generation of synthesis models, to  $\sim 35\%$ . Our technique for selecting AGB-dominated clusters in nearby galaxies promises to be effective for discriminating the uncertainties associated with AGB stars in intermediate-age populations that plague age and mass estimation in high- $z$  galaxies.

*Subject headings:*

## 1. INTRODUCTION

Light emitted from stars in the thermally-pulsing asymptotic giant branch (AGB) phase of stellar evolution has implications for our view of the baryonic content and chemical state of galaxies, both locally and at high redshift, from UV-to-mid-IR observations. Recent advances in modeling and observation have enhanced this perspective, especially regarding the dust formation and mass loss that accompanies the late (thermal pulsing) stages of AGB evolution (e.g. Groenewegen 2006; Jackson et al. 2007; Groenewegen et al. 2009; Boyer et al. 2011). These findings demonstrate the influential role AGBs play in the enrichment of the ISM with gas and dust (e.g. Srinivasan et al. 2009; Matsuura et al. 2009; Sargent et al. 2010) and place more accurate constraints on AGB lifetimes (i.e. Girardi & Marigo 2007).

However, our view of stellar populations as a whole

has only slowly incorporated this picture, and uncertainties in the ages and masses of intermediate-age systems remain. Because they are some of the brightest objects between ages 0.2-1 Gyr, a handful of AGB stars can outshine all other stars at rest-frame wavelengths  $\lambda \gtrsim 1 \mu m$  while contributing only minimally to the total mass. Accurate AGB models are therefore a critical ingredient in stellar population synthesis (SPS) techniques (Mouhcine & Lançon 2002; Bruzual & Charlot 2003; Maraston 2005; Charlot & Bruzual 2007; Gonzalez-Lopezlira 2010). But, even the latest generation of SPS models with an updated treatment of the AGB phase (e.g. Charlot & Bruzual 2007 with Marigo et al. 2008) rarely extend beyond  $3 \mu m$ , and few include the effect of extinction by the AGB star's circumstellar dust shell on the integrated properties of the stellar population (but see Mouhcine 2002).

Here we examine whether recent evidence in favor of a reduced NIR AGB contribution (Kriek et al. 2010) arises from the extinction of AGBs by their dusty envelopes. With a view extending from the optical to the mid-IR, we study a sample of AGB-dominated clusters in M100 selected for, and classified by, their dust emission. This avoids the challenges of optical or NIR detection and classification in the presence of the dust shell (e.g. van Loon et al. 2005) and supplies unique leverage on the role of dust to shift AGB light from the NIR to longer wavelengths.

## 2. THE DATA

We construct our sample of bright clusters in the disk of M100 ( $D=15.2$  Mpc; Freedman et al. 2001), chosen for its low inclination and the potential to probe a range of metallicities. Objects are selected based on their emis-

<sup>1</sup> Max-Planck-Institut für Astronomie / Königsstuhl 17 D-69117 Heidelberg, Germany

<sup>2</sup> National Radio Astronomy Observatory

<sup>3</sup> European Space Agency Research Fellow (ESTEC)

<sup>4</sup> The Observatories of the Carnegie Institution for Science

<sup>5</sup> Instituto de Astrofísica de Canarias, Spain

<sup>6</sup> Departamento de Astrofísica, Universidad de La Laguna, Spain

<sup>7</sup> Laboratoire d'Astrophysique de Marseille (LAM)

<sup>8</sup> University of Arizona

<sup>9</sup> Spitzer Science Center

<sup>10</sup> California Institute of Technology

<sup>11</sup> Space Telescope Science Institute

<sup>12</sup> Universidad Complutense Madrid

<sup>13</sup> European Southern Observatory

<sup>14</sup> University of Oulu, Finland

<sup>15</sup> Finnish Centre for Astronomy with ESO (FINCA), University of Turku

<sup>16</sup> Korea Astronomy and Space Science Institute

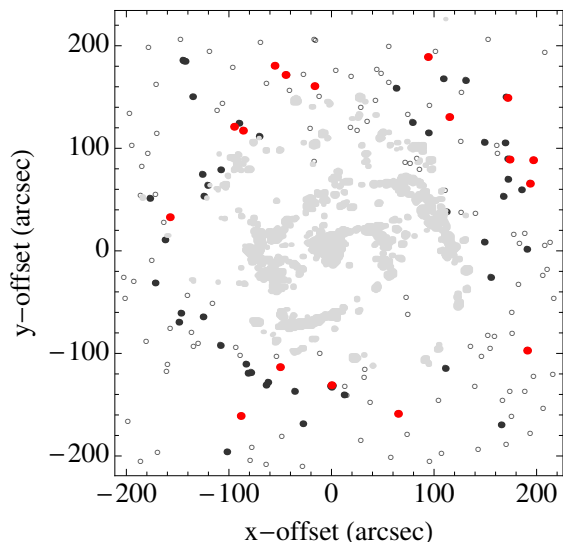


FIG. 1.— Spatial map of candidate clusters (open symbols), significant detections at  $\lambda \geq 1.2 \mu\text{m}$  (black) and the final sample (red), together with the hot dust/PAH emission (gray), separated as described in the text. Notice that PAH and hot dust emission more often appear in the high-density, actively star-forming regions.

sion in IRAC 3.6 and  $4.5 \mu\text{m}$  images processed by the S<sup>4</sup>G team (Sheth et al. 2010; see selection technique below). In order to sample the SED from 0.2 to  $24 \mu\text{m}$ , we supplement these data with archival BVRI data from SINGS (Dale et al. 2005; Dale et al. 2007) and SINGS IRAC 5.8 and  $8 \mu\text{m}$  and MIPS  $24 \mu\text{m}$  images (Kennicutt et al. 2003). We also include HAWK-I JHK imaging provided by P. Grosbol (e.g. Grosbol & Dottori 2011). A map of continuum-subtracted  $\text{H}\alpha$  from SINGS (Kennicutt et al. 2003; Calzetti et al. 2007) provides cross-check against HII regions/young embedded clusters.

Our cluster sample spans a large radial range in the disk, out to  $R \sim 200''$  (limited by the NIR field of view). Extrapolation of the measured gradient in the nebular emission-line chemical abundances (Moustakas et al. 2010) in M100 suggests that the ISM metallicity reaches  $12 + \log(\text{O}/\text{H}) \approx 8.1$  by  $R = 300''$ . Assuming little chemical evolution over the last  $\sim 1$  Gyr, this suggests that the cluster sample spans  $0.27 < Z/Z_{\odot} < 0.6$ . In what follows, we refer to radial position and metallicity synonymously.

### 2.1. Selection of cluster candidates

The identification of red clusters at 3.6 and  $4.5 \mu\text{m}$  is based on the Independent Component Analysis (ICA) of the images at these wavelengths (see Meidt et al. 2012). ICA separates the light from the oldest stars, with colors  $[3.6] - [4.5] < 0$ , from the emission contributed by contaminants, with colors  $0 < [3.6] - [4.5] \lesssim 1.5$ . Candidate bright red clusters, which fall into the second category, are distinguishable from the other main sources of contaminant emission at  $3.6 \mu\text{m}$  given the very different relation to the non-stellar emission  $F_{8,ns}$  at  $8 \mu\text{m}$ .

Using the selection criterion  $F_{3.6}/F_{8,ns} > 0.3$  to avoid emission from PAH and hot dust as advocated by Meidt et al. (2012), we generate a map of 172 candidate clusters, shown in Figure 1. This map is used to identify the cluster emission in all wavebands, including at 3.6 and  $4.5 \mu\text{m}$ .

### 2.2. Multiband Photometry

Photometric measurements for candidate clusters are extracted in circular apertures  $6''$  in radius, sized for compatibility with the  $6''$  PSF FWHM at  $24 \mu\text{m}$ , our lowest angular resolution image. For this aperture size, sampling a region 444 pc in radius at the distance of this galaxy, we adopt corrections to the infinite aperture of 1.05, 1.07, 1.08, 1.09 and 1.67 at 3.6, 4.5, 5.8, 8 and  $24 \mu\text{m}$ , respectively, for point sources (SSC IRAC Handbook Handbook; Reach et al. 2005) and assume that these corrections are small or negligible in the optical images (i.e. Dale et al. 2007; Calzetti et al. 2007). We have confirmed that smaller apertures yield similar flux measurements for  $\lambda < 24 \mu\text{m}$ .

To isolate the cluster light from the underlying disk in each aperture we subtract local background values measured in annuli spanning between  $r = 6''$  and  $12''$  with  $2\sigma_0$  clipping to avoid contamination by neighboring clusters. The variance in the local background value  $\sigma_0$  defines the uncertainty in the photometric measurement  $\sigma$  for each aperture, along with calibration and aperture correction uncertainties (added in quadrature). Calibration uncertainties are  $\sim 10\%$  in the NIR bands and below this level in the IRAC bands, at MIPS  $24 \mu\text{m}$  and in the optical (Dale et al. 2005), while aperture corrections are typically 10% uncertain in IRAC bands and  $< 5\%$  uncertain at  $24 \mu\text{m}$ .

## 3. PHOTOMETRIC PROPERTIES

### 3.1. Sample definition

Roughly half of the candidate clusters are detected in all bands longward of  $1 \mu\text{m}$ . Obscuration by dust presumably contributes to some non-detections in the NIR. To ensure a realistic signal we adopt thresholding at  $3\sigma$ . Measurement uncertainties for the remaining 80 significant detections are well below 20% (nearer 10% on average) and are omitted for the final sample in all upcoming plots for clarity.

Candidate clusters have some of the reddest colors in the shortest IRAC wavebands ( $0 < [3.6] - [4.5] < 1$ ; Meidt et al. 2012) consistent with the colors of AGB stars. Still, possible contaminants include background galaxies, quasars, and younger dust enshrouded clusters. Galaxy number counts over the range in  $3.6 \mu\text{m}$  magnitudes in our sample are high (e.g. Fazio et al. 2004, Sanders et al. 2007), but only a subset have  $[3.6] - [4.5]$  colors that can be confused with emission from dusty AGBs, namely quasars and the nearest and brightest background galaxies, for which the observed mid-IR colors are closest to rest-frame colors (e.g. Fazio et al. 2004). In the latter case, 14 are removed with a minimum size criterion (set by the  $3.6 \mu\text{m}$  FWHM), and 12 others avoided with limits to the mid-IR colors: star-forming galaxies will have  $[3.6] - [8] > 3.35$  (tracing hot dust and PAH emission) and  $[8] - [24] \gtrsim 2.4$  (see Boyer et al. 2011).

Contamination from background galaxies is otherwise naturally limited by the optically thick disk of M100 (Holwerda et al. 2005). As a secondary safeguard we use the few known background galaxies detected by Holwerda et al. (2005) between  $70''$  and  $140''$  in archival HST/WFPC2 imaging to construct a composite SED against which all candidates are compared. These galaxies are on average one magnitude dimmer at  $3.6 \mu\text{m}$  than clusters in our final sample and have  $\text{B-K} \gtrsim 3$ ,  $\text{K-[8]} \gtrsim 4$  and  $[3.6] - [8.0] \gtrsim 3$ . Note that sources falling nearest the disk

edge where the dust column density is lower show less strongly the suppression at optical wavelengths characteristic of foreground disk extinction. We therefore expect the above mid-IR color criteria to be a stronger limit for these.

According to the detection rate of AGN behind the LMC and SMC we expect quasar contamination to be minimal (less than 2 in the field studied here; Kozłowski & Kochanek 2009), and few candidates approach the limit  $R-K \sim 4$  used to detect obscured quasars with similar mid-IR colors (e.g. Lacy et al. 2004; Gilkman et al. 2007). Embedded star formation in young massive clusters and HII regions illuminating the surrounding dust are perhaps stronger potential contaminants. Our imposed criterion  $[3.6]-[8] < 3.35$  already avoids many such objects, 4 of which also have detectable  $H\alpha$  emission. To select against any more deeply embedded mid-IR bright clusters we impose a  $3\sigma$  threshold in the optical BVRI bands. With 27 such sources removed, the remaining 17 visually confirmed clusters exhibit  $[3.6]-[8]$  colors consistent with emission from circumstellar material (see Figure 2), as expected around AGB stars undergoing high mass loss (e.g. Groenewegen et al. 2009; Sargent et al. 2011; Srinivasan et al. 2011).

### 3.2. Sample description

By construction, selected clusters originate in zones with little to no emission from PAH and hot dust at 3.6 and 4.5  $\mu\text{m}$  and so they should also be largely removed of locations in the disk susceptible to the effects of reddening and extinction by diffuse dust (see Figure 1). Extra-cluster extinction is therefore expected to be minimal, especially since the final 17 clusters fall in the outer disk where the dust column density is low. As revealed in § 4.1, our mid-IR measurements are consistent with emission from the circumstellar dust shell produced, and illuminated, by the AGB star, itself, rather than from a diffuse dust component emitting re-processed radiation from cluster stars. We take the measured red B-V colors (Figure 2) as characteristic of intrinsically red objects with a spread in ages between 0.2-1 Gyr (Bruzual 2007; Mouhcine & Lançon 2002).

Our sample is evidently composed of coeval massive cluster complexes with  $M > 10^6 M_\odot$  (e.g. Trancho et al. 2007; referred to simply as clusters in what follows), given the unavoidable bias towards the brightest sources at this distance and our requirement for optical detections. The depth of the potential of the cluster complex relative to the shallow outer disk provides a natural way to avoid dispersal at these late ages (i.e. Fellhauer & Kroupa 2005), while interaction with the companion galaxy suggests a plausible seed for the formation of such massive complexes (e.g. Larsen 2004).

## 4. VARIATION IN THE AGB CONTRIBUTION

### 4.1. Distinction between O-rich, C-rich and extreme AGB stars

The varying degrees of circumstellar dust extinction expected around AGBs are potentially closely related to the chemistry of the star and the mass of its progenitor. C-rich stars will be more highly extinguished than O-rich stars for the same mass-loss rate, given the higher opacities of the carbonaceous grains produced in their

atmospheres (e.g. Suh 2000; Pégorié 1988; Mouhcine 2002). The highest levels of extinction occur in the extreme AGB phase, during which the star undergoes its highest mass-loss rates. Following Boyer et al. (2011), we use mid-IR colors to differentiate between clusters dominated by C-rich, O-rich or extreme AGB stars (Figure 2).

Although age and metallicity variations between clusters may introduce scatter relative to the separation in, e.g., the LMC (Boyer et al. 2011), the different AGB star types cleanly separate by their mid-IR colors. Note that, without spectral confirmation, these particular classifications are subject to interpretation. Following Kastner et al. (2008) and Groenewegen et al. (2009), for example, the xAGBs here would be classified as C-rich (and see Ferraro et al. 1995).

Clusters also show good correspondence with the NIR colors of isolated AGBs (top right panels of Figure 2), despite the higher contribution from the rest of the cluster members than in the mid-IR. These very red NIR colors supply additional confirmation that our clusters are dominated by AGBs undergoing high mass-loss rates (e.g. Gonzalez-Lopezlira 2010); even with the implied color excess  $E(B-V)$  for ages between 1-10 Myr, we find that the NIR colors remain consistent with 0.2-1.2 Gyr old clusters.

Our classifications are confirmed in the  $[8]-[24]$  vs. J-K diagram (middle; cf. Boyer et al. 2011). Based on this diagram our ‘mid-IR bright’ objects can be associated with the anomalously dusty O-rich (aO-rich) AGBs identified by Boyer et al. (2011). This is also favored by our combined optical and mid-IR view: where the red  $[3.6]-[8]$  colors of dust-reprocessed emission from young embedded clusters would coincide with dust-reddened B-V colors, these objects have some of the bluest optical colors in the sample. These objects may therefore be the O-rich counterpart to the extreme C-rich AGBs in our sample.

The bottom right panel of Figure 2 depicts the dependence of AGB type on mass and metallicity, in line with the mechanisms that influence the C/O ratio (see, e.g., van Loon et al. 2005). The dustiest AGBs notably sit in younger clusters, where AGB progenitors are of higher mass than at older ages. This accounts for the enhanced dust production in these stars, if the implied longer pulsation period for these high masses leads to higher mass-loss rates. In contrast, the less dusty C-rich and O-rich appear less often here and only at the outer radii as a result of our mid-IR and optical detection thresholds and large aperture.

### 4.2. Extinction in K band

The impact of the different AGB star dust chemistries and mass-loss rates is clear in Figure 3 where clusters form a sequence that becomes progressively redder in K-[8] color while becoming bluer in B-K color. The optical-NIR color traces the fractional flux contribution of AGB stars relative to the other (less evolved) cluster members, which dominate in the optical. The K-[8] color meanwhile serves to measure the amount of dust produced around the AGB stars, in the sense that enhanced 8  $\mu\text{m}$  dust emission and reduced K-band brightness due to extinction both drive reddening in K-[8].

To reproduce the downward trend in this color-color

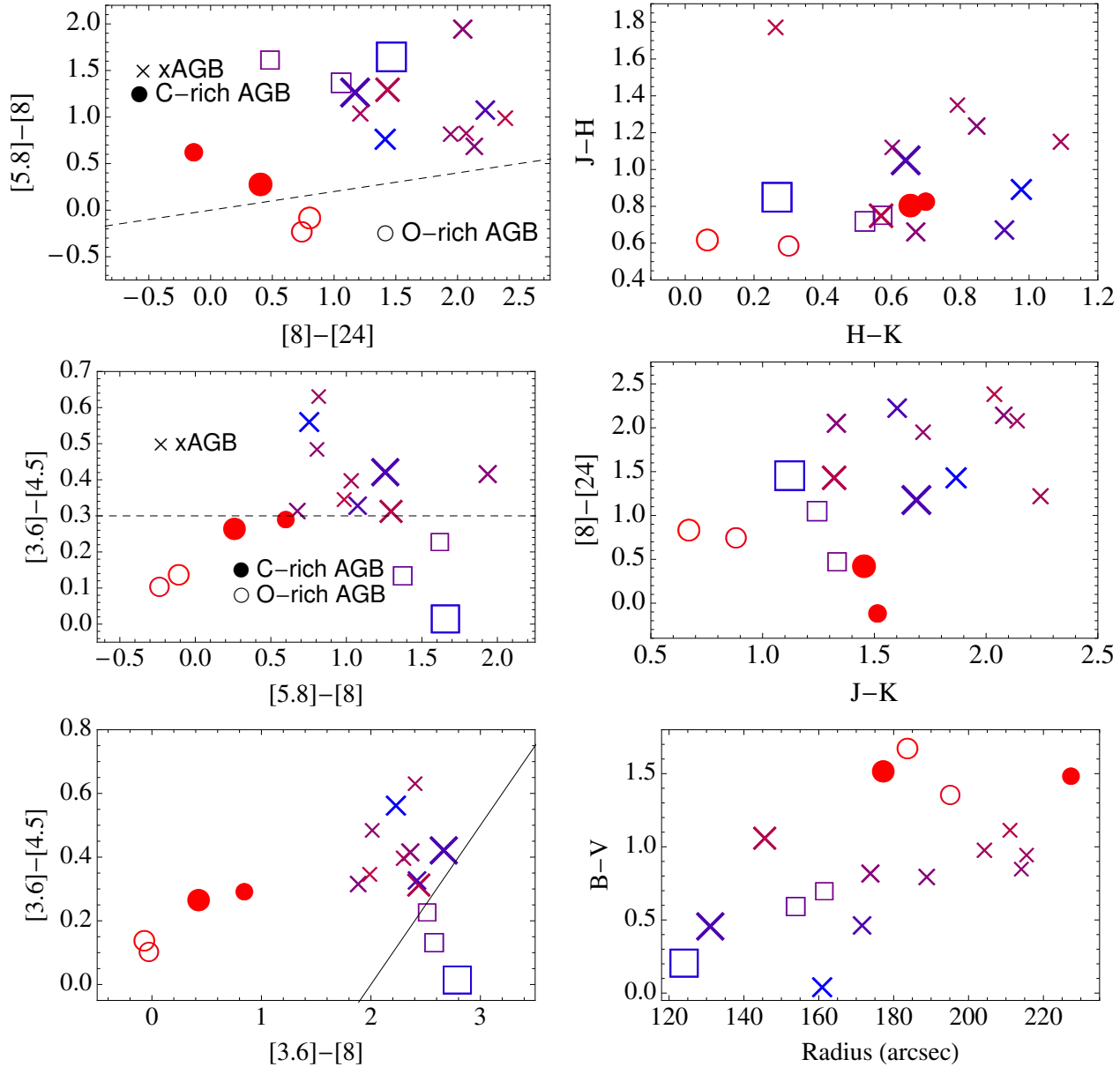


FIG. 2.— (*Left Column*) Separation between clusters hosting C-rich (closed), O-rich (open) or extreme (crosses) AGB stars. Dashed gray lines show our criteria for distinguishing between the three main types, as motivated by Boyer et al. (2011). Square symbols mark a fourth subset of ‘mid-IR bright’ objects to the left of the solid black line in the bottom panel, which could potentially be dusty young clusters (e.g. Corbelli et al. 2011), later classified in this work as anomalously dusty O-rich stars (see Figure 2). The color scaling represents variation in B-V color, from B-V=0 (blue) to B-V=1.5 (red), used as a proxy for cluster age, while the symbol size varies according to metallicity, from low (small) to high (large). (*Right Column*) (*Top*) J-H vs. H-K color for all objects in the sample. (*Middle*) [8]-[24] vs. J-K diagram as used by Boyer et al. (2011) to distinguish between dust chemistries. The aO-rich AGBs with silicate dust follow a nearly vertical sequence near J-K $\sim$ 1.3, while extreme C-rich AGBs are distributed more horizontally. (*Bottom*) Positions and B-V colors of our clusters tracking metallicity and cluster age, respectively.

diagram that separates the C-rich from the O-rich AGBs and the dustiest AGBs from those that are less dusty requires a decrease in the K-band cluster light from the top left to the bottom right (depicted by the overlaid dashed lines of K-band dimming at arbitrary fixed B and [8] brightness). This can be most easily explained by an enhanced obscuration of the AGB stars as the optical depth of their dust shells increase.

The stellar photosphere or spectral type of the AGB star also plays a role in determining the location within this diagram (e.g. Sargent et al. 2011). This is contained in our distinction between C-rich and O-rich chemistries and so, in this sense, it is largely indistin-

guishable from the implied dust extinction. As a result of the different properties of the dust grains produced in the atmospheres of C-rich and O-rich stars, the former will be relatively more obscured for the same mass-loss rate.

Other interpretations for the downward trend in Figure 3 are either less viable or precluded by construction. By avoiding sources with mid-IR emission from dust heated by young stars we have removed the potential that the bluer B-K colors arise at an age before the onset of AGBs, as well as the possibility that reddest K-[8] colors trace extracuster dust heated to higher temperatures.

In addition, the decrease in B-K is inconsistent with

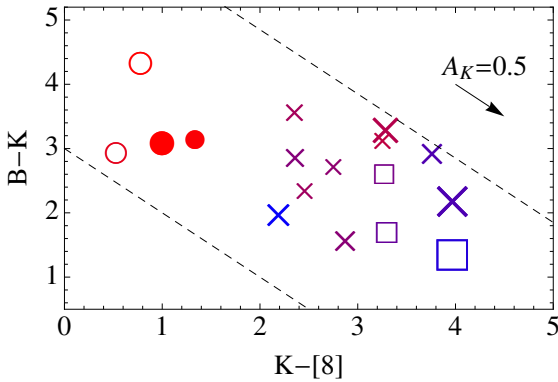


FIG. 3.— B-K vs. K-[8] color for the final cluster sample. Dashed lines illustrate decreasing K-band brightness at fixed B and  $8\ \mu\text{m}$  magnitudes. Symbol types, sizes and colors are as in Figure 2.

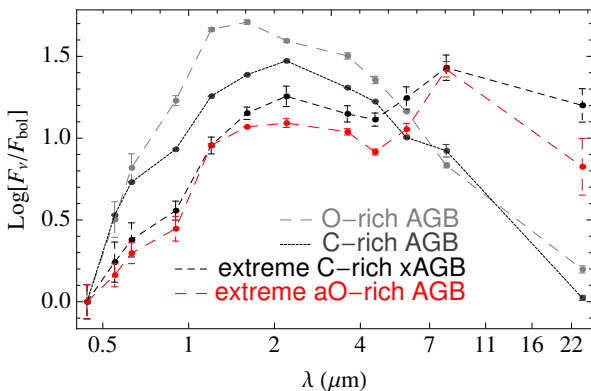


FIG. 4.— Composite SEDs normalized at  $0.4\ \mu\text{m}$ . For a given type, we take the average of SEDs each normalized to its bolometric flux  $F_{\text{bol}}$ . Error bars represent the dispersion in the measurements for each type.

fluctuations to lower AGB star number densities (resulting in lower NIR fluxes relative to the optical), as the corners of the diagram would also be filled, since B-K would be independent of K-8 in this case.

This trend is also not driven by intra-cluster dust from past mass loss by earlier AGBs at younger cluster ages, which would have reversed the observed red-to-blue progression in B-V colors along the downward sequence of increasing extinction. Instead, clusters that are blue in B-K are also blue in B-V. As noted in § 4.1, this reflects a genuine dependence on cluster age through the mass of the progenitor; at young cluster ages AGBs will evolve from higher mass stars resulting in AGBs with higher mass-loss rates and hence heavier extinction.

#### 4.3. Implications for age and mass estimation

The trend in Figure 3 implies that the contribution of dusty AGBs in K-band is much lower than expected from the B-band cluster emission due to circumstellar extinction. Since optical-NIR colors like B-K are commonly used as age indicators for intermediate-age populations (Bruzual 2007; Mouhcine 2002), this suggests that intrinsic extinction can significantly affect the predicted ages of AGB-dominated populations, as explored by Mouhcine (2002). Age estimation and classification from NIR colors should be likewise affected (e.g. Nowotny et al. 2011). More consequentially, models with relatively ‘bare’ AGBs, less extinguished by circumstellar

dust, will underpredict the stellar M/L for intermediate-age populations. This is demonstrated in Figure 4, showing composite SEDs for the four sets of clusters studied here, those that host O-rich and C-rich AGBs and those with relatively more obscured extreme C-rich and aO-rich AGBs. In the latter two cases, circumstellar dust clearly shifts the cluster emission from short to long wavelengths so that the NIR contribution of AGBs appears significantly lower than in the case of relatively ‘bare’ O-rich AGBs. The C-rich AGBs also shows a depression in the NIR relative to the O-rich case. This amounts to  $0.12\ \text{dex} \approx 0.3\ \text{mag}$  extinction in K-band for C-rich stars compared to O-rich stars and on average  $\sim 0.5\ \text{dex}$  extinction for the dustiest AGBs (or as much as 1 mag, also judging by the offset in B-K color in Figure 3).

The difference in SED shapes with and without strong AGB star extinction can explain the apparent compatibility found by Kriek et al. (2010) between the SEDs of post-starburst galaxies and the older generation of Bruzual & Charlot (2003) models, where AGBs contribute  $\sim 30\text{--}40\%$  in K at 1 Gyr rather than  $\sim 70\%$  in the recent, updated Bruzual & Charlot (2007) models. But the agreement found by Kriek et al. (2010) would seem to be largely coincidental: taking the extinction measured from difference in K-band light in the undimmed and dimmed cases, then a 70% contribution from AGB stars in K-band (30% from the cluster) will be reduced to  $\sim 35\%$  as the result of circumstellar dust extinction.

## 5. CONCLUDING REMARKS

We have presented evidence that the fractional contribution of AGBs to intermediate-age populations, a contentious prediction of stellar population synthesis models, is significantly affected by the presence of the dusty envelope produced during this stage. The extinction generated by dust shells around AGBs in  $\sim 1\ \text{Gyr}$  old clusters (on average  $0.5\ \text{mag}$ ) is sensitive to the type of AGB star: C-rich AGBs produce shells with higher optical depths than their O-rich counterparts and the high mass-loss rates of xAGBs lead to even higher obscuration. Consequently, population ages estimated from optical-NIR colors may be underestimated (as predicted by Mouhcine 2002) leading also to under-prediction of the stellar M/L. The range in circumstellar extinction revealed here may account for the fact that SPS models with very different AGB star contributions each seem to fit a diversity of observations well (cf. Maraston et al. 2006, van der Wel et al. 2006 and Kriek et al. 2010).

S.E.M. thanks Arjen van der Wel for discussion and Angela Adamo and Anibal Garcia for their helpful comments on the manuscript. E.A. and A.B. thank the Centre National d’Etudes Spatiales for financial support.

TABLE 1  
CATALOG OF AGB-DOMINATED CLUSTERS<sup>a</sup>

<sup>a</sup>All photometric measurements are presented relative to Vega.

ID	RA (deg)	DEC (deg)	$m_B$ (mag)	$dm_B$ (mag)	$m_V$ (mag)	$dm_V$ (mag)	$m_R$ (mag)	$dm_R$ (mag)	$m_I$ (mag)	$dm_I$ (mag)	$m_J$ (mag)	$dm_J$ (mag)	$m_H$ (mag)	$dm_H$ (mag)
1	185.7518	15.7765	21.158	0.103	19.503	0.101	17.987	0.100	16.842	0.100	14.918	0.050	14.312	0.050
2	185.709	15.7771	22.275	0.250	21.813	0.278	20.462	0.178	19.914	0.162	18.350	0.080	17.677	0.084
3	185.727	15.7849	21.667	0.135	21.215	0.153	20.770	0.176	20.241	0.145	18.573	0.072	17.526	0.073
4	185.741	15.7898	20.616	0.156	20.405	0.182	20.211	0.266	20.543	0.313	17.764	0.098	16.910	0.095
5	185.674	15.7942	21.308	0.106	20.467	0.103	19.414	0.102	18.893	0.104	17.708	0.052	16.591	0.054
6	185.771	15.8304	21.060	0.140	21.022	0.183	20.639	0.226	20.222	0.178	18.366	0.112	17.478	0.097
7	185.674	15.8395	22.149	0.120	21.175	0.110	19.951	0.108	20.044	0.119	18.217	0.054	17.065	0.064
8	185.679	15.846	19.739	0.100	18.393	0.100	17.151	0.100	16.603	0.100	15.093	0.050	14.512	0.050
9	185.673	15.8458	20.974	0.103	20.036	0.102	19.213	0.102	19.477	0.112	18.165	0.055	16.818	0.056
10	185.751	15.8538	21.258	0.270	20.197	0.167	19.199	0.140	18.725	0.115	16.672	0.060	15.922	0.060
11	185.754	15.8549	20.137	0.190	19.544	0.174	18.787	0.158	18.884	0.158	17.061	0.074	16.339	0.074
12	185.695	15.8575	20.330	0.106	19.520	0.106	18.797	0.106	18.923	0.108	17.497	0.061	16.837	0.062
13	185.68	15.8627	20.242	0.101	18.773	0.100	17.740	0.100	17.500	0.101	16.041	0.050	15.226	0.050
14	185.732	15.8659	19.969	0.158	19.262	0.138	18.163	0.117	17.887	0.109	16.074	0.053	15.316	0.053
15	185.74	15.8689	20.281	0.107	18.773	0.101	17.738	0.101	17.481	0.100	16.060	0.050	15.262	0.050
16	185.743	15.8714	21.781	0.111	20.994	0.111	19.964	0.108	20.352	0.126	18.411	0.057	17.180	0.063
17	185.701	15.8738	22.956	0.151	21.840	0.126	21.192	0.138	20.157	0.105	19.253	0.069	17.479	0.058
ID			$m_K$ (mag)	$dm_K$ (mag)	$m_{3.6}$ (mag)	$dm_{3.6}$ (mag)	$m_{4.5}$ (mag)	$dm_{4.5}$ (mag)	$m_{5.8}$ (mag)	$dm_{5.8}$ (mag)	$m_8$ (mag)	$dm_8$ (mag)	$m_{24}$ (mag)	$dm_{24}$ (mag)
1			14.247	0.050	13.400	0.112	13.270	0.112	13.360	0.113	13.468	0.116	12.664	0.079
2			16.748	0.068	15.408	0.116	15.080	0.115	14.063	0.122	12.987	0.125	10.762	0.072
3			16.885	0.065	15.583	0.114	15.164	0.113	14.175	0.123	12.918	0.125	11.747	0.076
4			16.643	0.100	15.465	0.130	15.448	0.132	14.332	0.160	12.676	0.157	11.212	0.081
5			15.988	0.052	15.250	0.112	14.768	0.112	14.043	0.115	13.236	0.114	11.290	0.071
6			16.500	0.071	16.538	0.149	15.979	0.126	15.064	0.161	14.310	0.257	12.894	0.109
7			15.972	0.061	15.917	0.114	15.521	0.115	14.653	0.124	13.619	0.118	12.404	0.080
8			14.212	0.050	13.656	0.112	13.555	0.112	13.447	0.113	13.684	0.119	12.945	0.087
9			16.026	0.054	15.974	0.114	15.344	0.113	14.386	0.120	13.570	0.117	11.498	0.072
10			15.352	0.057	14.503	0.114	14.190	0.113	13.361	0.121	12.066	0.131	10.632	0.073
11			15.817	0.067	15.098	0.121	14.964	0.120	13.892	0.123	12.518	0.123	11.462	0.078
12			16.166	0.057	15.655	0.118	15.242	0.115	15.231	0.139	13.294	0.116	11.251	0.072
13			14.525	0.050	14.036	0.112	13.750	0.112	13.788	0.114	13.189	0.114	13.324	0.094
14			14.741	0.052	13.985	0.113	13.755	0.113	13.091	0.119	11.470	0.121	10.988	0.078
15			14.606	0.050	14.037	0.112	13.776	0.112	13.868	0.116	13.608	0.131	13.202	0.103
16			16.331	0.068	15.858	0.114	15.546	0.115	14.649	0.122	13.973	0.135	11.836	0.075
17			17.216	0.056	15.953	0.114	15.608	0.115	14.949	0.132	13.962	0.122	11.574	0.072

## REFERENCES

- Boyer, M. L., Srinivasan, S. van Loon, J. et al. 2011, AJ, 142, 103  
 Bruzual G. & Charlot S., 2003, MNRAS, 344, 1000  
 Bruzual, G. 2007, in IAU Symposium 241 Stellar populations as building blocks of galaxies, eds. A. Vazdekis and R. Peletier, Cambridge: Cambridge University Press, 125  
 Calzetti, D. et al. 2007, ApJ, 666, 870  
 Corbelli, E., Giovanardi, C., Palla, F., Verley, S., 2011, A&A, 528, 116  
 Dale, D.A. et al. 2005, ApJ, 633, 857  
 Dale, D.A. et al. 2007, ApJ, 655, 863  
 Fazio, G. G., Ashby, M. L. N., Barmby, P., Hora, J. L., Huang, J.-S., Pahre, M. A. Wang, Z., Willner, S. P., Arendt, R. G., Moseley, S. H., Brodwin, M., Eisenhardt, P., Stern, Daniel, Tollestrup, E. V. & Wright, E. L. 2004, ApJSS, 154, 39  
 Fellhauer, M. & Kroupa, P. 2005, ApJ, 630, 879  
 Ferraro, F. R. et al. 1995, MNRAS, 272, 391  
 Freedman, W.L. et al. 2001, ApJ, 553, 47  
 Gilkman, E., Helfand, D. J., White, R. L., Becker R. H., Gregg, M. D. & Lacy, M. 2007, ApJ, 667, 673  
 Girardi, L. & Marigo, P. 2007, A&A, 462, 237  
 Gonzalez-Lopezlira, R. A., Bruzual, G., Charlot, S., Ballesteros-Paredes, J. & Loinard, L. 2010, MNRAS, 403, 1213  
 Groenewegen, M. A. T. 2006, A&A, 448, 181  
 Groenewegen, M. A. T., Sloan, G. C., Soszynski, I., & Petersen, E. A. 2009, A&A, 506, 1277  
 Grosbol, P. & Dottori, H. 2011, arXiv:1109.4255  
 Holwerda, B. W., Gonzalez, R. A., Allen, R. J. & van der Kruit, P. C. 2005, AJ, 129, 1396  
 Jackson, D. C., Skillman, E. D., Gehrz, R. D., Polonski, E. & Woodward, C. E. 2007, ApJ, 656, 818  
 Kastner, J. H. et al. 2008, AJ, 136, 1221  
 Kennicutt, Jr., R. C., et al. 2003, PASP, 115, 928  
 Kozłowski, S. & Kochanek, C. S. 2009, ApJ, 701, 508  
 Kriek, M. et al. 2010  
 Lacy, M., Storrie-Lombardi, L. J., Sajina, A., et al. 2004, ApJSS, 154, 166  
 Lagadec, E., Mekarnia, D., de Freitas Pacheco, J. A., Dougados, C., 2005, A&A, 433, 553  
 Lagadec, E. & Zijlstra, A. A. 2008, MNRAS, 390, L59  
 Larsen, S. S. 2004, A&A, 416, 537  
 Marigo, P., Girardi, L., Bressan, A., Groenewegen, M. A. T., Silva, L., & Granato, G. L. 2008, A&A, 482, 883  
 Maraston, C. 2005, MNRAS, 362, 799  
 Maraston, C. et al. 2006, ApJ, 652, 85  
 Matsuura, M. et al. 2009, MNRAS, 396, 918  
 Meidt, S. E., Schinnerer E., Knapen, J. H. et al. 2012, ApJ, 744, 17  
 Mouhcine, M. 2002, A&A, 394, 125  
 Mouhcine, M. & Lançon, A. 2002, A&A, 393, 149  
 Moustakas, J., Kennicutt, R. C., Tremonti, C. A., Dale, D. A., Smith, J.-D., T. & Calzetti, D. 2010, ApJS, 190, 233  
 Muñoz-Mateos, J. C. et al., 2009, ApJ, 701, 1965  
 Nowotny, W., Aringer, B., Hoefner, S. & Lederer, M.T. 2011, A&A, in press  
 Pégourié, B. 1988, A&A, 194, 335  
 Reach, W. T., et al. 2005, PASP, 117, 978  
 Sanders, D. B., Salvato, M., Aussel, H., et al. 2007, ApJS, 172, 86S  
 Sargent, B. A., Srinivasan, Meixner, M., et al. 2010, ApJ, 716, 878  
 Sargent, B. A., Srinivasan, S. & Meixner, M. 2011, ApJ, 728, 93  
 Sheth, K. et al. 2010, submitted to PASP  
 Srinivasan, S. et al. 2009, AJ, 137, 4810  
 Srinivasan, S. Sargent, B. & M. Meixner 2011, A&A, 532, A54

- Suh, K. -W. 2000, MNRAS, 315, 740
- Trancho, G. Bastian. N., Miller, B. W., & Schweizer, F. 2007, ApJ, 664, 284
- van der Wel, A., Franx, M., Wuyts, S., van Dokkum, P. G., Huang, J., Rix, H.-W., Illingworth, G. D. 2006, ApJ, 652, 97
- van Loon, J. T., Marshall, J. R., & Zijlstra, A. A. 2005, A&A, 442, 597